

# 4-1BB agonist targeted to fibroblast activation protein $\alpha$ synergizes with radiotherapy to treat murine breast tumor models

Eneko Garate-Soraluze <sup>1</sup>, Irantzu Serrano-Mendioroz,<sup>1</sup> Leticia Fernández-Rubio,<sup>1</sup> Carlos E De Andrea,<sup>2</sup> Celia Barrio-Alonso <sup>3</sup>, Claudia del Pilar Herrero,<sup>2</sup> Alvaro Teijeira <sup>1</sup>, Carlos Luri-Rey,<sup>1</sup> Christina Claus,<sup>4</sup> Tamara Tanos,<sup>4</sup> Christian Klein <sup>4</sup>, Pablo Umana,<sup>4</sup> Antonio Rullan,<sup>5</sup> Jon Ander Simón,<sup>6</sup> María Collantes,<sup>6</sup> Paloma Sánchez-Mateos,<sup>3</sup> Ignacio Melero <sup>1,7,8,9,10</sup> Maria E Rodriguez-Ruiz <sup>1,8,9,10</sup>

**To cite:** Garate-Soraluze E, Serrano-Mendioroz I, Fernández-Rubio L, *et al.* 4-1BB agonist targeted to fibroblast activation protein  $\alpha$  synergizes with radiotherapy to treat murine breast tumor models. *Journal for ImmunoTherapy of Cancer* 2025;**13**:e009852. doi:10.1136/jitc-2024-009852

► Additional supplemental material is published online only. To view, please visit the journal online (<https://doi.org/10.1136/jitc-2024-009852>).

Accepted 01 November 2024



© Author(s) (or their employer(s)) 2025. Re-use permitted under CC BY-NC. No commercial re-use. See rights and permissions. Published by BMJ Group.

For numbered affiliations see end of article.

## Correspondence to

Dr Maria E Rodriguez-Ruiz; mrruiz@unav.es

## ABSTRACT

**Background** Ionizing radiation (IR) is a double-edged sword for immunotherapy as it may have both immunosuppressive and immunostimulatory effects. The biological effects of IR on the tumor microenvironment (TME) are a key factor for this balance. Fibroblast activation protein (FAP) is expressed on the surface of cancer-associated fibroblasts (CAF) in many cancer types and its abundance is associated with the poor immune response to immune-checkpoint-blockade in patients. We hypothesized that IR increases FAP expression in CAFs, therefore the combination of IR with targeted immunomodulators such as an agonistic anti-FAP-4-1BBL fusion protein could enhance the immune-mediated antitumoral effects of these treatments.

**Methods** The murine transplantable TS/A tumor-cell-line co-engrafted with CAFs was used to investigate increases in FAP expression in tumors following irradiation using immunohistochemistry, real-time polymerase chain reaction (RT-PCR) and multiplex tissue immunofluorescence. One lesion of bilateral tumor-bearing mice was only locally irradiated or combined with weekly injections of the bispecific muFAP-4-1BBL fusion protein (a mouse surrogate for RG7826). Tumor sizes were followed over time and TME was assessed by flow cytometry. Selective monoclonal antibody (mAb)-mediated depletions of immune cell populations, neutralizing interferon alpha/beta receptor 1 (IFNAR-1) IFNAR and interferon (IFN)- $\gamma$  mAbs and gene-modified mice (4-1BB<sup>-/-</sup>) were used to delineate the immune cell subsets and mechanisms required for efficacy. <sup>67</sup>Ga labeled muFAP-4-1BBL tracked by SPECT-CT was used to study biodistribution. In human colorectal carcinoma samples, the inducibility of FAP expression following radiotherapy was explored by multiplex immunofluorescence.

**Results** Irradiation of TS/A+CAF tumors in mice showed an increase in FAP levels after local irradiation. A suboptimal radiotherapy regimen in combination with muFAP-4-1BBL attained primary tumor control and measurable abscopal effects. Immune TME landscape analyses showed post-treatment increased infiltration

## WHAT IS ALREADY KNOWN ON THIS TOPIC

⇒ Cancer-associated fibroblast (CAF) are one of the main constituents of tumor microenvironment. Fibroblast activation protein (FAP) is largely expressed within this protumoral cell subset and have shown to induce immunotherapy resistance in solid tumors. Radiotherapy is known to exert proinflammatory as well as antitumoral responses in tumors.

## WHAT THIS STUDY ADDS

⇒ This study demonstrates local tumor control of radiotherapy in combination with bispecific muFAP-4-1BBL antibody fusion protein in breast tumor models together with observable abscopal responses and improved with the addition of programmed cell death protein-1 (PD-1) and cytotoxic T-lymphocyte associated protein 4 (CTLA-4) blockade. The antitumoral response is CD8<sup>+</sup> T cell and 4-1BB expression dependent and improved tumor targeting than its counterpart is observed, due to FAP binding moiety. In vivo findings are replicated in human patients with colorectal.

## HOW THIS STUDY MIGHT AFFECT RESEARCH, PRACTICE OR POLICY

⇒ Obtained preclinical results warrant clinical testing of the above-mentioned radioimmunotherapy strategy, which has confirmed safety in advanced solid tumors (R07122290). In addition, FAP-targeting antibodies in combination with radiotherapy hold promise for a new radioimmunotherapy strategy.

of activated immune cells associated with the combined radioimmunotherapy treatment. Efficacy depended on CD8<sup>+</sup> T cells, type I IFN, IFN- $\gamma$  and ability to express 4-1BB. Biodistribution studies of muFAP-4-1BBL indicated enriched tumor targeting to irradiated tumors. Human colorectal cancer samples pre and post irradiation showed enhanced FAP expression after radiotherapy.

**Conclusion** Increased FAP expression in the TME as a result of radiotherapy can be exploited to target agonist 4-1BB immunotherapy to malignant tumor lesions using an FAP-4-1BBL antibody fusion protein.

## INTRODUCTION

Cancer-associated fibroblasts (CAFs) are recognized as one of the stromal cellular constituents of the tumor microenvironment in most solid tumors.<sup>1–3</sup> Elevated levels of infiltrating CAFs within tumor tissues are commonly linked to unfavorable prognosis and treatment outcomes.<sup>4</sup> In contrast to normal tissue fibroblasts, CAFs play a crucial role in promoting cancer progression through the secretion of various soluble paracrine factors, including growth factors, cytokines chemokines and extracellular matrix components.<sup>5–7</sup> These factors not only regulate the behavior of neighboring cancer cells but also regulate the recruitment of inflammatory and immune cells, as well as bone marrow-derived progenitor cells.<sup>8</sup> Multiple lines of evidence suggest that the tumor stroma profoundly influences tumor immunity and responses to immunotherapy.<sup>9</sup> While CAFs are traditionally believed to exert pro-inflammatory and immunosuppressive functions within tumors, recent studies based on single-cell RNA sequencing (scRNA-seq) have challenged this notion, suggesting that different subsets of CAFs may play opposing roles and, contextually, may even support antitumor immune responses.<sup>10</sup>

Fibroblast activation protein (FAP) is a surface serine protease predominantly expressed in activated fibroblasts and CAFs. FAP expression has been identified as a leading marker to identify activated CAFs across various solid cancer types including colorectal cancer,<sup>11–13</sup> breast cancer<sup>14 15</sup> and melanoma.<sup>16</sup> Given the ubiquitous presence of CAFs within tumors and their supportive role for cancer cells, targeting CAFs has emerged as a promising anticancer strategy.<sup>17 18</sup> In recent years, considerable interest has been directed toward targeting tumor tissue using anti-FAP antibodies given the fact that FAP expression is low elsewhere in healthy organisms. Numerous bispecific constructs of FAP-targeted antibodies, coupled with co-stimulatory molecules such as, but not limited to CD40, 4-1BBL, and IL-2, have exhibited promising preclinical outcomes and have entered clinical trials.<sup>19–21</sup> These therapeutic agents aim to stimulate immune cells and redirect them to the tumor stroma, thereby enhancing pre-existing endogenous immune responses against tumor cells.<sup>22</sup>

Ionizing radiation in the clinical setting affects both malignant and non-malignant elements of the tumor microenvironment (TME), thus eliciting cancer-cell extrinsic responses to treatment.<sup>23</sup> While some studies suggest an immunosuppressive effect of CAFs within the TME following radiotherapy (RT),<sup>24 25</sup> others have proposed a conversion of CAFs into a more immune-stimulating stromal population.<sup>10</sup> Given its low-level expression in normal tissue, FAP represents an attractive target for selectively delivering potent immunostimulatory

molecules in which non-targeted delivery can pose systemic toxicity issues.<sup>26 27</sup> In this study, we investigate the combination of RT and the bispecific muFAP-4-1BBL antibody fusion protein, a mouse-reactive surrogate molecule for FAP-4-1BBL (RG7826),<sup>28</sup> comprised of a monovalent FAP-specific targeting arm and a dimeric mu4-1BBL (online supplemental figure 1), to investigate its effects on achieving CD8<sup>+</sup> T cell-mediated local and partial abscopal tumor growth control.

## MATERIAL AND METHODS

### Mice

6-week-old female BALB/c mice were procured from Harlan Laboratories (Barcelona, Spain) and housed at the Centro de Investigacion Medica Aplicada (CIMA, Pamplona, Spain) animal facility. 4-1BBLKO and MMTV-Neu mice were bred at CIMA. The experimental protocols were approved by the Ethics Committee of the University of Navarra (CEEA037-20 and CEAAE27-23) in accordance with European Council Guidelines.

### Cell lines

The TS/A mouse breast carcinoma cell line was generously provided by Dr Lorenzo Galuzzi (Weill Cornell Medical College, New York, New York, USA). The BALB/c-derived 4T1 breast carcinoma cell line was originally obtained from Dr Claude Leclerc (Institute Pasteur, Paris, France) and validated in the master cell bank at the Institute Pasteur (Paris, France). The TS/A cell line was cultured in DMEM+GlutaMAX (Gibco) supplemented with 10% fetal bovine serum (FBS), 1% penicillin-streptomycin (Life Technologies) and 50 μM 2-mercaptoethanol (Gibco). 4T1-mCherry and 4T1 cell lines were cultured in RPMI 1640 GlutaMAX (Gibco) supplemented with 10% FBS, 1% penicillin-streptomycin (Life Technologies) and 50 μM 2-mercaptoethanol (Gibco). The CAF cell line was established from isolated CAFs from MMTV-Neu mice tumors and cultured in a CAF medium (see online supplemental material). Cell lines were cultured under standard conditions (5% CO<sub>2</sub>, 37°C under humidity) and routinely tested every 2 months for *Mycoplasma* contamination using the MycoAlert Mycoplasma Detection Kit (Lonza).

### Tumor models

For the 4T1-mCherry unilateral tumor model, 3×10<sup>5</sup> cells were subcutaneously injected into the right flank on day 0 in a volume of 50 μL. For TS/A+CAF bilateral tumor model, 1.5×10<sup>5</sup> TS/A cells mixed with 5×10<sup>5</sup> CAFs were subcutaneously co-injected into the right flank, while 0.75×10<sup>5</sup> TS/A cells mixed with 2.5×10<sup>5</sup> CAFs were co-injected into the left flank of 8–10-week-old female BALB/c mice. In case of CAF-GFP<sup>+</sup> co-injection, 1.5×10<sup>5</sup> TS/A cells mixed with 5×10<sup>5</sup> CAF-GFP<sup>+</sup> were subcutaneously co-injected in one flank. The ratio (1:3.33) of tumor cells to CAFs was maintained between the primary and contralateral tumors (CTs). Tumor measurements were performed

twice a week with calipers. When the tumors reached a volume of 80–100 mm<sup>3</sup> or 120–140 mm<sup>3</sup> (immune checkpoint experiment), the mice were randomized into different experimental treatment groups. For tumor rechallenge, tumor-free mice up to 90 days were subcutaneously injected with 5×10<sup>5</sup> TS/A and 5×10<sup>5</sup> 4T1 cells in the right and left flank, respectively.

### In vivo experiments

To determine the local and abscopal effects, primary tumor (PT)-bearing mice received intraperitoneal injections of 3 mg/kg muFAP-4-1BBL (P1AE8721, F.Hoffmann-La Roche) or the untargeted control muDP47-4-1BBL (PIAG3059, F.Hoffmann-La Roche) once per week for 5 weeks (online supplemental figure 1), with or without hypofractionated focal irradiation (6 Gy×2 fractions) of the PT but not the CT. RT was delivered using the Small Animal Radiation Research Platform (Xstrahl) for TS/A, TS/A+CAF-GFP<sup>+</sup> and 4T1-mCherry tumors, when volumes ranged between 80 and 100 mm<sup>3</sup> or for immune checkpoint blockade experiment, when tumor volumes ranged between 120 and 140 mm<sup>3</sup>. Tumor growth was monitored every 2–3 days, and the mice were sacrificed when the tumor size reached 2000 mm<sup>3</sup>. Programmed cell death protein-1 (PD-1) and cytotoxic T-lymphocyte associated protein 4 (CTLA-4) blockade therapy was provided by intraperitoneal injection of 200 µg of anti-PD-1 (clone RMP1-14, Bio X Cell) and anti-CTLA-4 (clone 9D9, Bio X Cell) on days 11, 15, 18, 22, 25, and 29, and on days 9, 12, and 15, respectively. Control mice received intraperitoneal injections of rat and mouse IgG, respectively. In some experiments, BALB/c mice deficient in 4-1BB or their wild-type counterparts were used.

### In vivo depletion of CD4, CD8 T cells, and neutralization of interferon- $\gamma$ and interferon- $\alpha$

For immune cell depletion studies, 100 µg of anti-mouse CD4 rat IgG2b (clone GK1.5) and CD8a rat IgG2b (clone 2.43), 500 µg of anti-mouse interferon (IFN)- $\gamma$  rat IgG1 (clone XMG1.2), and control rat IgG monoclonal antibodies were administered on days 7, 14, and subsequently every week. Blood samples were taken during the experiment and analyzed by flow cytometry to confirm complete depletion of the corresponding lymphocyte subset, or ELISA was performed to ensure IFN- $\gamma$  depletion. For IFN- $\alpha$  depletion studies, anti-mouse IFN- $\alpha$  receptor mouse IgG1 (clone MAR1-5A3) or control mouse IgG were intratumorally administered to treated tumors on days 7, 8, 9, 10 and 11. Blood samples were taken during the experiment, and tumors were excised for ELISA and real-time polymerase chain reaction (RT-PCR) analysis, respectively, to confirm IFN- $\alpha$  neutralization.

### Mouse immunohistochemistry assay

For immunohistochemical detection of FAP or CD8, TS/A+CAFs-derived tumors were frozen in optimal cutting temperature compound (Thermo Fisher Scientific) and cut into 10 µm sections. Slides were dried

for 30 min at room temperature, fixed in cold acetone and washed once with tris buffered saline (TBS). After washing, slides were blocked with 0.3% H<sub>2</sub>O<sub>2</sub> for 30 min and incubated overnight at 4°C with detection rabbit antibody specific for anti-mouse FAP rabbit IgG (1:500, clone 28H1, (P1AE8721), F.Hoffmann-La Roche) or CD8 $\alpha$  (98941, 1:100, Cell Signaling). Following incubation with the detection antibody, slides were washed with TBS and incubated for 1 hour with EnVision+System HRP labeled polymer anti-Rabbit (Dako). Finally, slides were washed again, revealed with DAB (3,3'-Diaminobenzidine from Dako) and stained with hematoxylin (RE7107, Leica Biosystems). Slides were scanned with the Aperio CS2 scanner (Leica Biosystems) and images were visualized with the Aperio Image Scope. Image analysis was performed on the whole tumor region from each slide using the open-source digital pathology software QuPath V.4.2. Traditional phenotyping approach by thresholding on the histogram of mean signal intensity was used to determine the FAP-positive and CD8-positive cells. Then, the percentage of positive cells in total cells was calculated for each slide (see online supplemental material).

### Mouse immunofluorescence multiplex assay

Tumor cryosections were fixed with cold acetone for 10 min, stained with different antibodies and analyzed by confocal microscopy. For fibroblast phenotyping, samples were stained with anti-mouse FAP rabbit IgG (clone 28H1, F.Hoffmann-La Roche), anti- $\alpha$ SMA (Novus Biologicals A249895, clone SPM332), anti-collagen type VI (Abcam ab51824, clone ER-TR7) and anti-GFP (Thermo Fisher Scientific #A-11120, clone 3E6) antibodies. Donkey anti-rabbit Cy3 (#711-166-152, Jackson Immunology), Goat anti-Mouse IgG1 Alexa Fluor 488 (#A-21121, Thermo Fisher), Donkey anti-rat Alexa Fluor 647 (#712-606-150, Jackson Immunology) and Goat anti-Mouse IgG2a Alexa Fluor 647 (#A-21241, Thermo Fisher) were used as secondary antibodies. All quantifications were performed in 3–5 20× fields and 2–4 regions of interest (ROI) were analyzed within each sample. Imaging was performed using the glycerol ACS APO 20× NA0.60 immersion objectives of a confocal fluorescence microscope (SPE, Leica-Microsystems). FIJI software was used for fibroblast segmentation of collagen type VI expressing cells using the analyze particle tool (minimum size of 15 µm<sup>2</sup>). The mean fluorescence intensity of FAP and  $\alpha$ SMA was measured for each segmented fibroblast, and the median value was used to determine the high expression of FAP or  $\alpha$ SMA in CAFs.

### Human multiplex immunofluorescence staining and analyses

Multiplex immunofluorescence staining and analysis was performed as previously described on a Bond RX auto-stainer.<sup>29 30</sup> Four-microns-thick formalin-fixed paraffin-embedded (FFPE) tissue sections were deparaffinized (Bond Dewax, Leica Biosystems) and rehydrated per standard protocols. Antigen retrieval was performed with Bond Epitope Retrieval Solution 1 (ER1, Leica

Biosystems) or 2 (ER2, Leica Biosystems), followed by four sequential cycles of staining with each cycle including a 30 min combined block and primary antibody incubation (Akoya antibody diluent/block), followed by a secondary HRP-conjugated polymer. Signal amplification was achieved with TSA-Opal fluorophores. Between cycles of staining, tissue sections underwent heat-induced epitope retrieval to remove the primary/secondary-HRP antibody complexes before staining with the next antibody. The primary antibodies and corresponding fluorophores are polyclonal anti-human CD3 rabbit antibody (ready-to-use, Agilent IR503) in Opal 480; anti-human CD8 mouse IgG1 (clone C8/144B, ready-to-use, Agilent GA62361-2) in Opal 520; anti-human FAP rabbit IgG (clone SP325, 1:50 dilution, Abcam) in Opal 690; and anti-cytokeratin (CK) mouse IgG1 (clone AE1/AE3, ready-to-use, Leica Biosystems, NCL-L-AE1/AE) in Opal 780. We counterstained nuclei with Spectral DAPI (Akoya Biosciences, FP1490) and mounted the stained tissues with ProLong Diamond Antifade Mounting Medium (Thermo Fisher Scientific). The stained slides were scanned using the PhenoImager HT Automated Quantitative Pathology Imaging System (Akoya Biosciences). After image acquisition, unmixing of the spectral libraries was performed with inForm software (Akoya Biosciences). Unmixed images were then imported into the open-source digital pathology software QuPath V.0.4.4 for stitching, cell segmentation and cell phenotyping. For baseline biopsies, whole tumor regions from each slide were analyzed. For post-CRT resections, a pathologist selected around five ROIs (each ROI:  $0.3345\text{mm}^2$ ) of the tumor bed and five ROIs of peritumoral tissue. Each group of ROIs to cover around  $1.65\text{mm}^2$  of tissue. Marker expression was used to identify tumor cells expressing CK, T-cell population expressing CD3, cytotoxic T cells ( $\text{CD3}^+\text{CD8}^+$ ), and CAFs ( $\text{FAP}^+$ ). The densities of each cell population were quantified and expressed as the number of cells per  $\text{mm}^2$ .

### TRAM RNA sequencing analysis

To analyze the transcriptome, freshly harvested tumors were collected 48 hours after RT. RNA was extracted with RNA Easy Midi Kit (Qiagen) following the manufacturer's instructions and sent to Macrogen for RNA sequencing (RNA-seq). RNA-seq data analysis was performed using the following workflow: (1) the quality of the samples was verified using FastQ software

(<https://www.bioinformatics.babraham.ac.uk/projects/fastqc/>) and the trimming of the reads with trimomatic<sup>31</sup>; (2) alignment against the mouse reference genome (GRCm39) was performed using STAR<sup>32</sup>; (3) gene expression quantification using read counts of exonic gene regions was carried out with featureCounts<sup>33</sup>; (4) the gene annotation reference was Gencode vM33<sup>34</sup>; and (5) differential expression statistical analysis was performed using R/Bioconductor. Data are publicly available in the gene expression omnibus (GEO) database with the accession number GSE255242. First, gene expression data was normalized with edgeR<sup>35</sup> and voom.<sup>36</sup>

After quality assessment and outlier detection using R/Bioconductor, a filtering process was performed. Genes with read counts lower than six in more than 50% of the samples of all the studied conditions were considered as not expressed in the experiment under study. Linear models for microarray data (LIMMA) was used to identify the genes with significant differential expression between experimental conditions. Further functional and clustering analyses and graphical representations were performed using R/Bioconductor and clusterProfiler.<sup>37</sup>

### Flow cytometry

To obtain unicellular cell suspensions, tumors were incubated in collagenase/DNase A (Roche) for 15 min at  $37^\circ\text{C}$  followed by mechanical disruption and passed through a  $70\ \mu\text{m}$  cell strainer (BD Falcon, BD Bioscience) by pressing with a plunger. Single-cell suspensions were treated with FcR-Block (anti-CD16/32 clone 2.4G2, BD Biosciences) in a phosphate-buffered saline (PBS)-based buffer containing 10% fetal calf serum to avoid unspecific staining. For surface staining fluorochrome-labeled antibodies, CD4-BUV496 (clone GK1.5, BD Bioscience), CD8-BUV395 (clone 53-6.7, BD Bioscience), CD25-APC R700 (clone PC61, BD Bioscience), CD45-BUV661 (clone 30-F11, BD Bioscience), PD-1-BV785 (clone 29F.1A12, BioLegend), 4-1BB-Biotin (clone 17B5, BioLegend), Streptavidin-PE/Dazzle (BioLegend), CD11c-FITC (clone N418, BioLegend), MHC-II-APCeFluor 780 (clone M5/114.15.2, Invitrogen) and CD86-BV510 (clone GL1, BD Bioscience) were used. For intracellular FoxP3-PeCy7 (clone FJK-16S, Invitrogen) staining, cells were first fixed and permeabilized for 30 min using the True-Nuclear Transcription Factor Buffer Set (BioLegend).

For ex vivo stimulation assay, lymphocytes from tumors were cultured with phorbol myristate acetate  $1\ \mu\text{g}/\text{mL}$  and ionomycin  $100\ \text{ng}/\text{mL}$  for 4 hours. GolgiPlug ( $1\ \mu\text{L}/\text{mL}$  cell culture BD Biosciences) was added to the culture medium as well as to the following reagents used during the staining. Single-cell suspensions were treated with FcR-Block (anti-CD16/32 clone 2.4G2, BD Biosciences) in a PBS-based buffer containing 10% FBS to avoid unspecific staining. For surface staining fluorochrome-labeled antibodies, CD4-BUV496 (clone GK 1.5, BD Bioscience), CD8-BUV395 (clone 53-6.7, BD Bioscience), CD45-BUV661 (clone 30-F11, BD Bioscience) were used. For intracellular granzyme B-FITC (clone NGZB, eBioscience) and Ki67-BV421 (clone 11F6, BioLegend) staining, cells were first fixed and permeabilized for 30 min using the BD Cytotfix/Cytoperm (BD Biosciences). For cell viability PromoFluor (Promocell) was used.

For CAF staining, tumors were first incubated with collagenase DNase P (Roche) and incubated at  $37^\circ\text{C}$  three times for 15 min while sequential pipetting. TrypLE Express Enzyme (Gibco) was added for additional disruption, and passed through a  $70\ \mu\text{m}$  cell strainer (BD Falcon, BD Bioscience) by pressing with a plunger. For surface staining, CD90.2-PB (clone 30-H12, BioLegend), CD45.2-PerCPCy5.5 (clone 104, BioLegend), CD31-PerCPCy5.5

(clone MEC13.3, BioLegend), Epcam-PerCPCy5.5 (clone G8.8, BioLegend), unlabeled anti-FAP rabbit IgG (clone 28H1, P1AE8721, F.Hoffmann-La Roche),  $\alpha$ SMA-PE (clone SPM332, Novus Biologicals) were used. As a secondary antibody for FAP staining, anti-Rabbit IgG-BV510 was used. For cell viability Zombie NIR (BioLegend) was used.

Samples were acquired in a CytoFLEX Flow cytometer (BD Biosciences) and CytExpert software was used for data analysis.

#### muFAP-4-1BBL/muDP47-4-1BBL radiolabeling

muFAP-4-1BBL (clone 28H1, P1AE8721, F.Hoffmann-La Roche) and the untargeted control muDP47-4-1BBL (P1AG3059, F.Hoffmann-La Roche) were adjusted to pH 8 by buffer exchange with a G-25 column (Cytiva, Fisher Scientific) using an elution buffer of 0.1 M NaHCO<sub>3</sub>. Following incubation at 37°C for 1 hour with a fivefold molar excess of the chelator p-NCS-benzyl-NODAGA (CheMatech, France). Excess of the chelator was eliminated by molecular exclusion using a 0.25 M sodium acetate solution supplemented with 5 mg/mL of gentisic acid. The day after, 185 MBq of gallium-67, (gallium chloride), was diluted to a volume of 200  $\mu$ L with 1M HCl, and added to an 800  $\mu$ L of the NODAGA-conjugated antibody solution (approximately 1.2 mg of antibody). The mixture was incubated at room temperature, obtaining a radiochemical yield of around 33%. Finally, free gallium-67 was removed by size exclusion purification and concentrated with an Amicon 30K.

#### Human samples

We selected matching archival biopsies (baseline biopsies) from patients with colorectal carcinoma who underwent preoperative chemoradiotherapy (CRT) followed by surgery at our institute. During this surgery, post-CRT FFPE specimens were collected and therefore available for use in this study. All patients signed informed consent forms for their tissues to be used in this study (general informed consent, V.3.3, February 7, 2019, under ethical protocol code 2010.111 mod4).

The CRT regimen included four cycles of capecitabine and oxaliplatin with concurrent 45 Gy in 25 fractions for 4 weeks, followed by resection. The recovery time interval between CRT and surgery was 4–6 weeks in surgical patients (19). All patients (12 patients) underwent standard surgery including total mesorectal excision. The clinical response after CRT and surgery was evaluated by endoscopy and MRI, and was then graded as complete response, partial response, no change, or residual disease based on the degree of histopathological tumor regression following the Guidelines for the Clinical and Pathological Studies on Carcinoma of the Colorectum. Only specimens from complete responders and residual disease were used. FFPE specimens cut in 10  $\mu$ m sections were stained.

#### Statistical analysis

Statistical analyses were performed using Prism software (GraphPad Prism V.6). One-way analysis of variance

(ANOVA) tests with Bonferroni post-test analysis, two-way ANOVA tests with Bonferroni post-test analysis, t-test when appropriate to determine statistical significance. Used tests are indicated in the figure legends. The Mantel-Cox test was used for survival analysis. Values of  $p < 0.05$  (\*),  $p < 0.01$  (\*\*) and  $p < 0.001$  (\*\*\*) were considered significant.

## RESULTS

### Irradiation induces FAP expression in transplanted mouse tumors

Following the hypothesis that irradiation could upregulate FAP expression on TME, a tumor model, rich in CAF was generated by subcutaneously co-engrafting breast cancer TS/A cell line (low-level FAP expression) with isolated CAFs from MMTV-Neu spontaneous breast cancer mouse model. After cell inoculation, as shown in [figure 1A](#), tumors were irradiated with two consecutive microenvironment-modulating doses (6 Gy/2 fractions), and surgically harvested on days 15 and 16. CAF density enrichment was observed in the TME together with enhanced FAP and  $\alpha$ SMA presence after irradiation ([figure 1B–E](#) and online supplemental figure 2) as compared with control non-irradiated tumors. In addition, immune cell infiltration was analyzed and increased CD8<sup>+</sup> T-cell infiltration was observed after tumor irradiation ([figure 1D](#)).

In order to decipher the origin of FAP increased expression and study the dynamics of exogenous (inoculated) CAFs, CAF-GFP<sup>+</sup> were co-injected with TS/A and tracked in vivo (online supplemental figure 3A). First, co-engraftment was confirmed at day 7 by GFP detection within tumor. Following tumor irradiation, at day 18, a decrease of exogenous CAFs (CAF-GFP<sup>+</sup>) was observed together with a more abundant presence of endogenous CAFs (FAP<sup>+</sup>/GFP<sup>-</sup>) (online supplemental figure 3B) when compared with control non-irradiated tumors. These results suggest that local irradiation gives rise to the recruitment of new FAP<sup>+</sup> CAFs into the tumor lesions as ascertained by increased  $\alpha$ SMA<sup>+</sup> and FAP<sup>+</sup> cells in the TME. muFAP-4-1BBL synergizes with RT to treat irradiated tumors and this combination partially controls distant non-irradiated concomitant tumors

As local irradiation increased FAP expression, we hypothesized that it could increase the efficacy of a bispecific FAP-4-1BBL antibody fusion protein in vivo. Cell inoculation was followed by two RT doses of 6 Gy and intraperitoneal administrations of muFAP-4-1BBL once a week as indicated in [figure 2A](#). At the primary irradiated tumors, we observed a better tumor control for RT+muFAP-4-1BBL as compared with monotherapy with muFAP-4-1BBL or a combination with a non-targeted 4-1BBL which was used as a negative control (RT+DP47-4-1BBL). In addition, the FAP-targeted combination regimen showed a significant reduction in the volumes of concomitant CTs that were not irradiated ([figure 2B and D](#)). As a consequence, overall survival was improved in mice treated with the

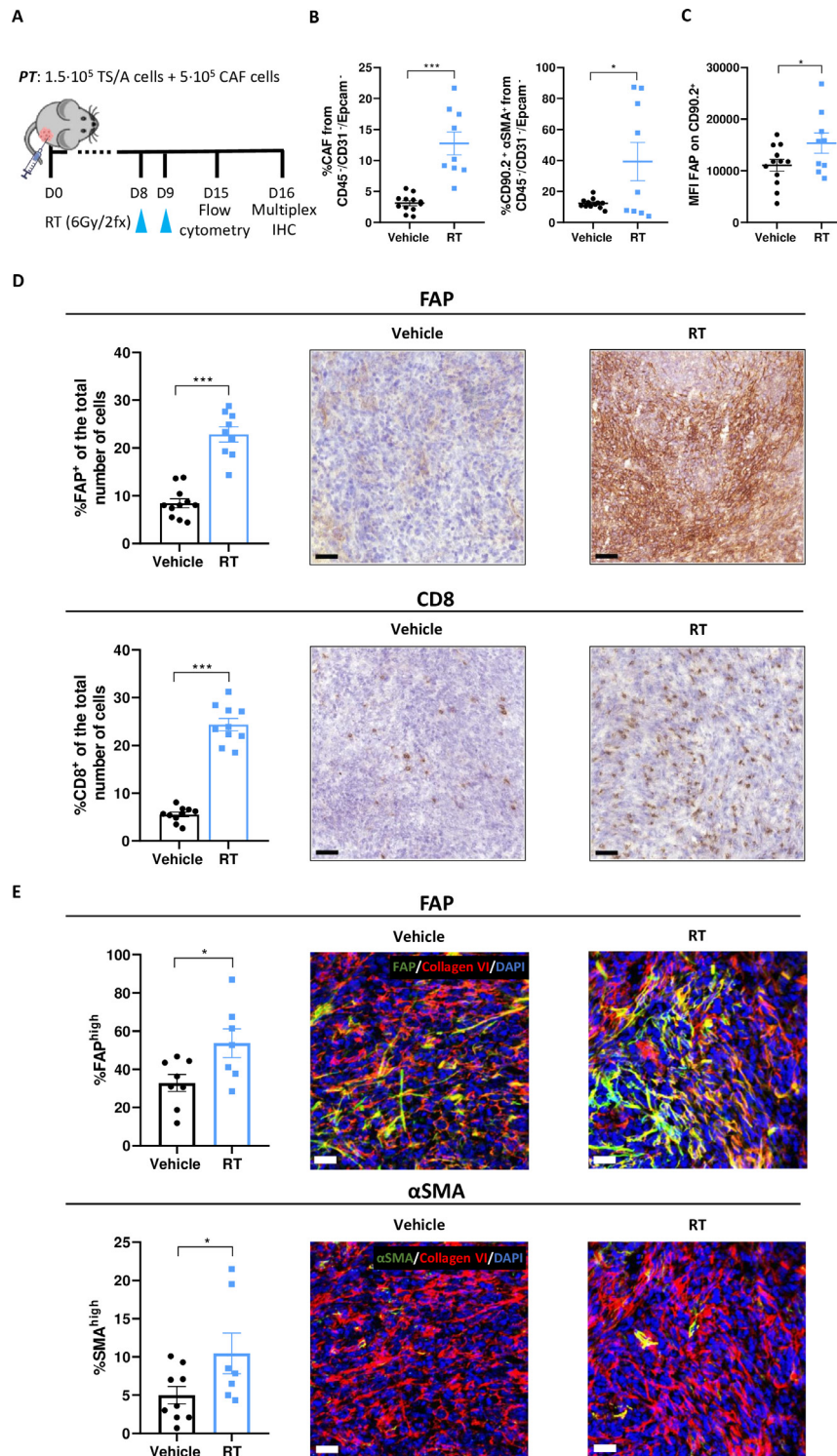


**Figure 1** Irradiation increases the presence of FAP<sup>+</sup> fibroblasts in engrafted mouse tumors. (A) Scheme of TS/A+CAF co-injection followed by hypofractionated radiotherapy (RT, blue arrows) of the primary tumor (PT) but not a contralateral tumor. Subsequent immunohistochemistry (IHC), flow cytometry and multiplex studies were performed at the indicated days (n=7–9 mice/group). (B) Non-treated (vehicle) and irradiated (RT) tumors were compared in TS/A+CAF model. Shown are the frequency in % of CAF (CD90.2<sup>+</sup> in the total population of CD45<sup>-</sup>/CD31<sup>-</sup>/Epcam<sup>-</sup>) and the frequency in % of CAF  $\alpha$ SMA<sup>+</sup> quantification by flow cytometry of the digested tumor. (C) Median fluorescence intensity (MFI) of FAP on CAFs (n=9–11 mice/group). (D) IHC studies of FAP expression and CD8<sup>+</sup> T-cell immune infiltration. Representative images (50  $\mu$ m). (E) Multiplex immunofluorescence in non-treated (vehicle) and irradiated (RT) tumors showing markers: FAP, collagen type VI,  $\alpha$ SMA. The nuclei were counterstained with DAPI. Plots, representative images and their single staining (50  $\mu$ m) (n=7–11 mice/group). Results show means $\pm$ SEM, each symbol indicates one mouse, significance is analyzed by one-tailed t-test, \*p<0.05, \*\*\*p<0.001. Pooled data from two independent experiments. CAF, cancer-associated fibroblast; FAP, fibroblast activation protein.

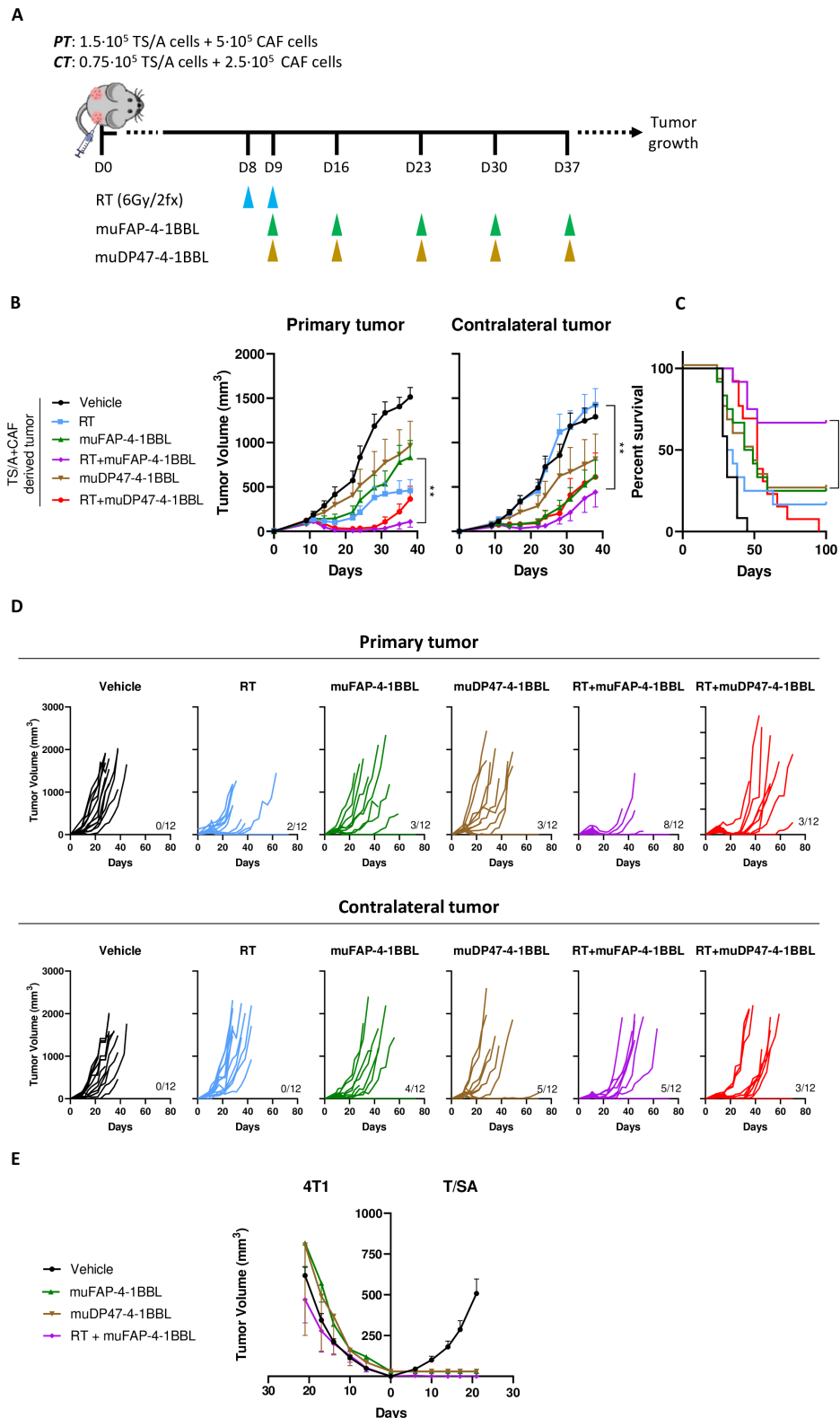


**Figure 2** muFAP-4-1BBL synergizes with local radiotherapy exerting partial abscopal control of non-irradiated distant tumors. (A) Scheme of 8-day TS/A+CAF co-injection and subsequent treatments with hypofractionated radiotherapy (RT, blue arrows) of the primary tumor (PT) but not contralateral tumor (CT). Tumor-bearing mice were treated by intraperitoneal administration of muFAP-4-1BBL (green arrows) or DP47-4-1BBL (brown arrows) and tumor size was monitored (n=12 mice/group). Pooled data from two independent experiments. (B) Tumor volumes ( $\text{mm}^3$ ) over time are shown per group as means $\pm$ SEM and statistical comparisons among experimental groups \*p<0.05, \*\*p<0.01, (two-way analysis of variance). (C) The percentage of survival over time is shown for the experiment (Mantel-Cox test). (D) Individual tumor sizes in the treated and distant non-irradiated tumors as indicated. (E) Rechallenge of cured mice is shown by 4T1 and TS/A cell line inoculation. CAF, cancer-associated fibroblast; FAP, fibroblast activation protein.



RT+muFAP-4-1BBL combination (figure 2C). Furthermore, rejections on rechallenge of cured mice with the same cell line confirmed the generation of long-term immunity (figure 2E).

Similar results were observed with tumors derived from the 4T1-mCherry breast cancer cell line, in which metastases spontaneously occur in the lungs. Orthotopic tumors were established (online supplemental figure 4A), and lungs were excised on day 34 to quantify metastases by RT-PCR of the gp70 antigen. The combination therapy targeted to FAP achieved better tumor control than RT+DP47-4-1 BBL as well as a lower burden of metastatic disease to the lungs (online supplemental figure 4B-D). These results confirmed the increased efficacy of combining RT with muFAP-4-1BBL.

### The effects of muFAP-4-1BBL combined with radiotherapy are dependent on CD8<sup>+</sup> T cells, 4-1BB, IFN type I and IFN- $\gamma$

To address the immune cell populations responsible for the therapeutic efficacy of RT and muFAP-4-1BBL, selective depletion studies of different immune cell subsets or selective cytokine neutralization with monoclonal antibodies (mAbs) were performed. Following the experimental setting in figure 3A, results showed the requirement of CD8<sup>+</sup> T cells as well as of IFN- $\gamma$  (figure 3B), whereas CD4<sup>+</sup> T-cell depletion improved response, suggesting a deleterious regulatory T cell (Treg) involvement, these results are consistent with previous reports.<sup>38</sup> IFN-I signaling, one of the downstream induced mediators of RT also appeared to be critical for the efficacy of the combination, as shown by antibody neutralization of interferon alpha/beta receptor 1 (IFNAR-1) (figure 3C-D). In addition, the antitumor effect was abrogated in knock-out mice lacking the 4-1BB gene (figure 3E-F). These results confirm that the therapeutic efficacy of the RT+muFAP-4-1BBL combination relies on the presence of CD8 T cell, the functionalities of type I and II IFNs as well as on the ability of T cells to express 4-1BB, which is the costimulatory target for the bispecific fusion protein.

### Irradiation and muFAP-4-1BBL favorably reshape the immune tumor microenvironment

We used flow cytometry on tumor cell suspensions to explore the changes in immune cell populations in the TME driven by the RT+muFAP-4-1BBL combination (figure 4A). The absolute numbers of Tregs, CD8<sup>+</sup> and CD4<sup>+</sup> T cells increased significantly in both the irradiated primary and non-irradiated CTs (figure 4B). As a result, higher numbers of 4-1BB<sup>+</sup> CD8<sup>+</sup> T cells and PD-1<sup>+</sup> CD8<sup>+</sup> T cells are observed in the combination group. In addition, cytotoxic phenotype markers, such as granzyme B and Ki67, showed a trend towards upregulation in CD8<sup>+</sup> T cells in the combination therapy group after stimulation with tumor cells (online supplemental figure 5A). We also observed a trend for dendritic cell increases together with enhanced expression of the dendritic cell (DC) activation marker CD86 after irradiation (figure 4C). Not only immune populations

within TME but also proinflammatory cytokines were upregulated in PT by the combination therapy (online supplemental figure 5B). Bulk RNA-seq of tumor tissue validated these results denoting a clear upregulation of T-cell infiltration and cytokines as well as genes related to cytotoxicity and IFN-I response in the combination therapy as compared with RT monotherapy (figure 4D and online supplemental figure 5C). Together with that, a pathway enrichment analysis was consistent with the other parameters showing a stimulation of antitumoral immune responses with RT+muFAP-4-1BBL combination (figure 4E).

We performed an IFN- $\gamma$  enzyme-linked immunosorbent spot (ELISpot) ELISpot assay to see if the combination therapy enhanced antigen-specific CD8-mediated adaptive immunity. As one of the most immunodominant antigens of TS/A is gp70, we incubated splenocytes from treated mice with gp70<sub>421-431</sub> (SPSYVYHQF) (online supplemental figure 6A). After splenocyte stimulation (online supplemental figure 6B-C), the combination therapy group showed the highest numbers of splenocytes capable of IFN- $\gamma$  release on antigen recognition. This data demonstrates that the combination of RT+muFAP-4-1BBL therapy leads to a more intense antitumor-specific response mediated by T cells.

### Irradiation enhances muFAP-4-1BBL targeting into irradiated tumor

As the activity of the bispecific construct relies on FAP binding, we sought to study the biodistribution of the antibody by labeling the protein construct with a radionuclide (<sup>67</sup>Ga) and tracking it over time by scintigraphy. Radiolabeled (<sup>67</sup>Ga)-muFAP-4-1BBL was administered and its biodistribution was monitored (figure 5A). Comparing non-irradiated and irradiated PTs, (<sup>67</sup>Ga)-muFAP-4-1BBL selectively accumulated in the tumor as shown by SPECT/CT images (figure 5B). These results were replicated when the accumulated antibody was measured in excised tumors (figure 5C). Hence RT induced FAP expression contributes to the targeting of 4-1BB costimulation to the immune tissue microenvironment.

In addition, we performed an experiment with a radiolabeled non-targeted 4-1BB agonist ((<sup>67</sup>Ga)-muDP47-4-1BBL) to see the biodistribution of the untargeted molecule as compared with the FAP-targeted 4-1BBL (online supplemental figure 7A). As shown in online supplemental figure 7B-D, liver accumulation of muDP47-4-1BBL was observed compared with its FAP-targeted counterpart. Notably, transaminase levels were not elevated following muDP47-4-1BBL administration in 4T1-mCherry engrafted mice (online supplemental figure 7E). Therefore, the differences in liver accumulation may be attributed to the FAP-targeting capacity of muFAP-4-1BBL rather than variations in tracer properties.

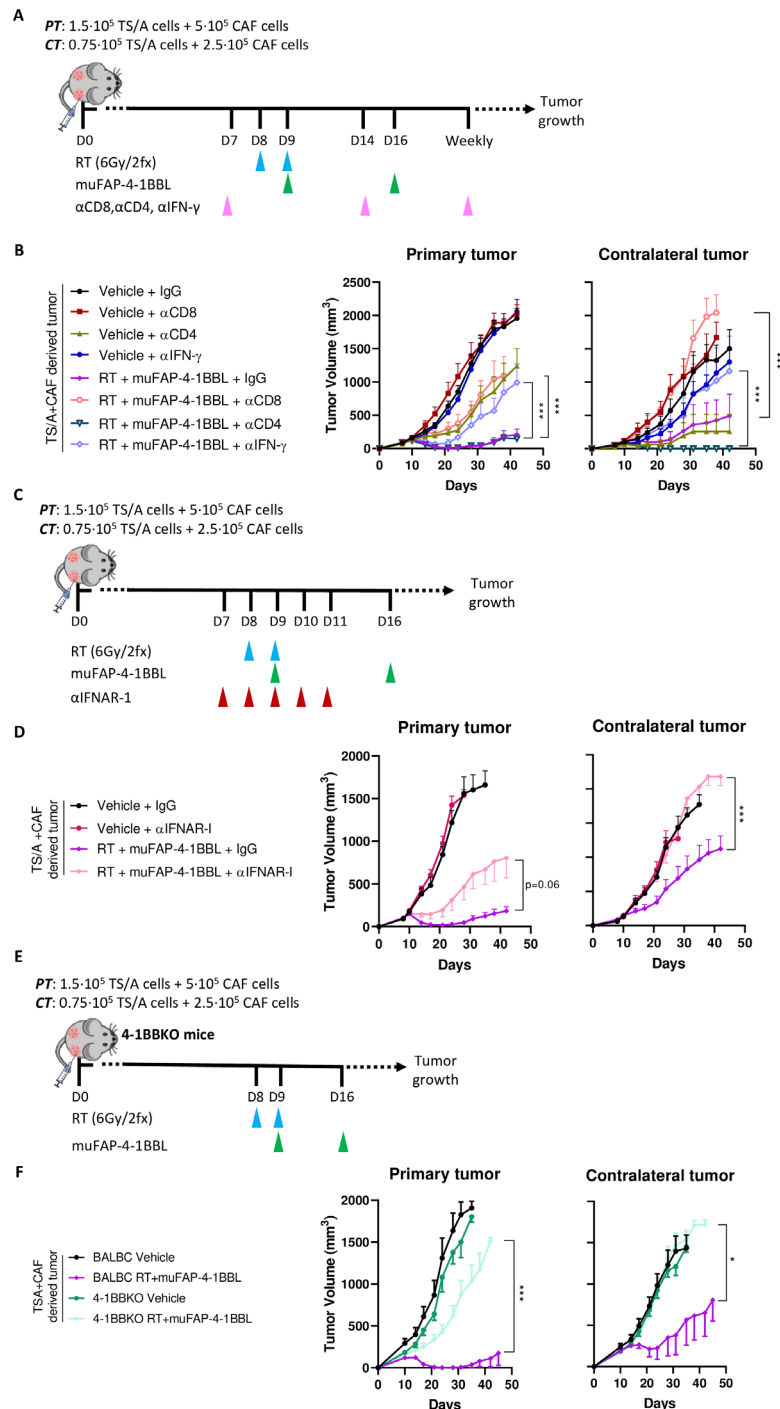


**Figure 3**  $CD8^+$  T cells, 4-1BB gene-integrity and the functions of type I and II IFNs are necessary for the synergistic therapeutic effects of RT+muFAP-4-1BBL. (A) Scheme of selective depletion of  $CD8^+$ ,  $CD4^+$  T cells and  $IFN-\gamma$  (pink arrows) in mice bearing bilateral TSA+CAFs-derived tumors in which primary tumors (PT) were treated with radiotherapy (RT, blue arrows) but not contralateral tumors (CT). Intraperitoneal administration of muFAP-4-1BBL (green arrows) was given as a combination therapy as indicated. (B) Tumor volumes ( $mm^3$ ) over time are shown per color-coded group as means $\pm$ SEM and compared (Two-way ANOVA) ( $n=9-12$  mice/group). Pooled data from two independent experiments. (C) Scheme of IFNAR blockade (red arrows) by intratumoral administration in mice bearing bilateral TSA+CAFs-derived tumors in which PT was treated with RT (blue arrows). Some mice received additional intraperitoneal administration of muFAP-4-1BBL (green arrows) as combination therapy. (D) Tumor volumes ( $mm^3$ ) over time are shown per color-coded group as means $\pm$ SEM (two-way ANOVA) ( $n=9-12$  mice/group). Pooled data from two independent experiments. (E) Scheme of 8-day tumor co-enuftment and subsequent treatments with hypofractionated radiotherapy (blue arrows) and intraperitoneal injections of muFAP-4-1BBL (green arrows) in bilateral subcutaneous TSA+CAF-derived tumors in 4-1BBKO mice. Tumor size was monitored over time. BALBc wildtype mice were treated similar as control. (F) Tumor volumes ( $mm^3$ ) over time are shown per color-coded group as means $\pm$ SEM (two-way ANOVA) ( $n=6-10$  mice/group). Significance is indicated as \* $p<0.05$ , \*\*\* $p<0.001$ . ANOVA, analysis of variance; CAF, cancer-associated fibroblast; FAP, fibroblast activation protein; IFN, interferon; IFNAR-I, interferon alpha/beta receptor 1.

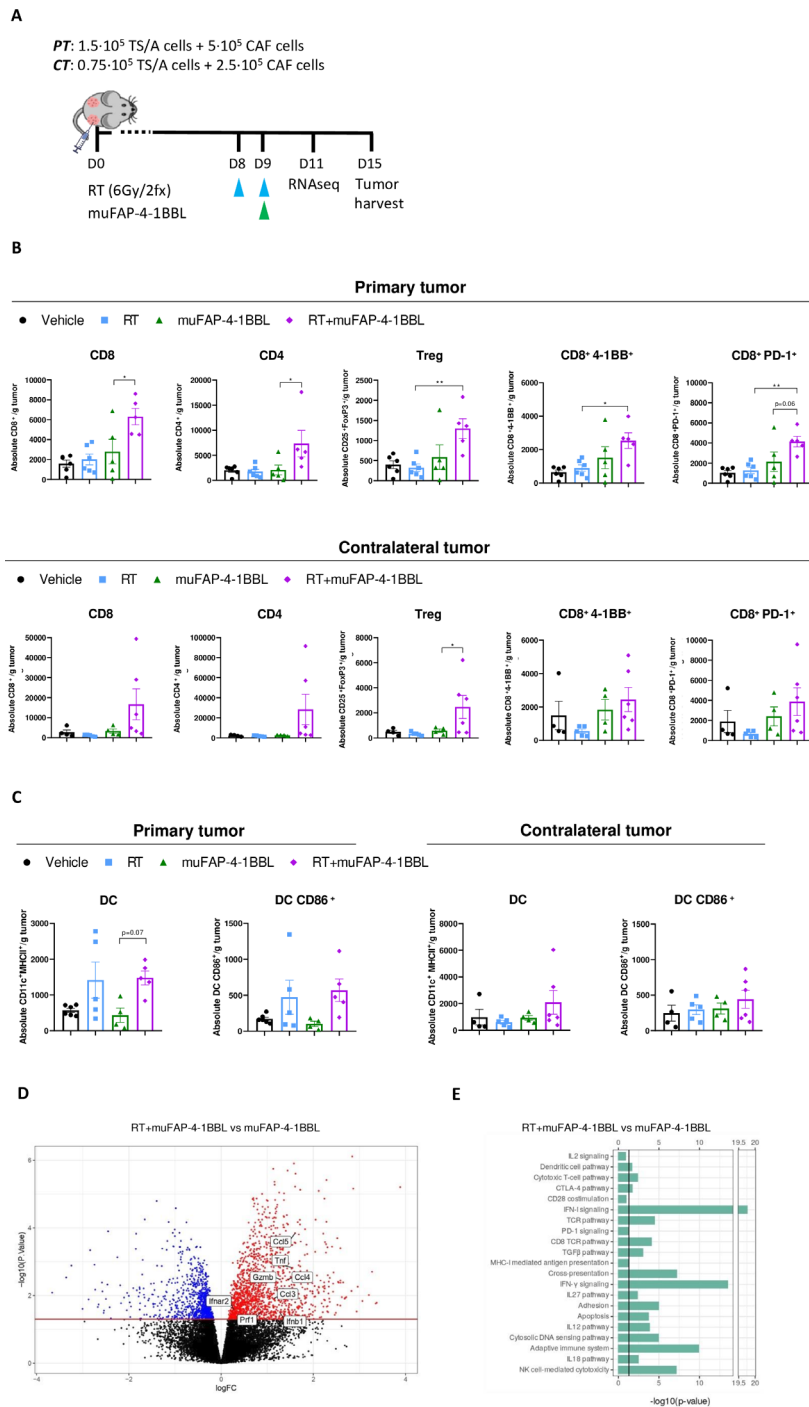


**Figure 4** Irradiation and muFAP-4-1BBL reshape the tumor microenvironment into a more immune-stimulating landscape. (A) Scheme of TS/A+CAFs tumor co-engraftment and subsequent treatments with hypofractionated radiotherapy of the primary tumor (RT, blue arrows) but not the contralateral tumor (CT). Intraperitoneal administration of muFAP-4-1BBL (green arrow) was given as combination therapy and tumors were excised at day 11 (RNA sequencing) and day 15 (flow cytometry analysis). (B) Plots showing the absolute numbers of the indicated T cells and their surface markers in primary (top panels) and contralateral (bottom panels) tumors analyzed by flow cytometry and normalized to gram of tumor. Each symbol indicates one mouse, mean $\pm$ SEM is indicated (two-way ANOVA). (C) Plots showing the absolute numbers of dendritic cells and their surface marker in primary and contralateral tumors analyzed by flow cytometry and normalized to gram of tumor ( $n=4-6$  mice/group). Each symbol indicates one mouse, mean $\pm$ SEM is indicated (two-way ANOVA) \* $p<0.05$ , \*\* $p<0.01$ , \*\*\* $p<0.001$ . (D) Volcano plot comparing the most upregulated ( $\log_{2}FC >4$ ) and downregulated genes ( $\log_{2}FC <-4$ ) at day 11 analyzed by RNA sequencing, whereby comparison was done between RT+muFAP-4-1BBL and muFAP-4-1BBL. Some of the most upregulated genes are highlighted by gene name. (E) Bar plots of p values presenting enrichment of immune-related pathways between RT+muFAP-4-1BBL and muFAP-4-1BBL. The vertical line shows the threshold value at  $p=0.05$ . Three mice of each treatment group were analyzed as indicated. ANOVA, analysis of variance; CAF, cancer-associated fibroblast; DC, dendritic cell; FAP, fibroblast activation protein; PT, primary tumor; RT, radiotherapy; Treg, regulatory T cell.

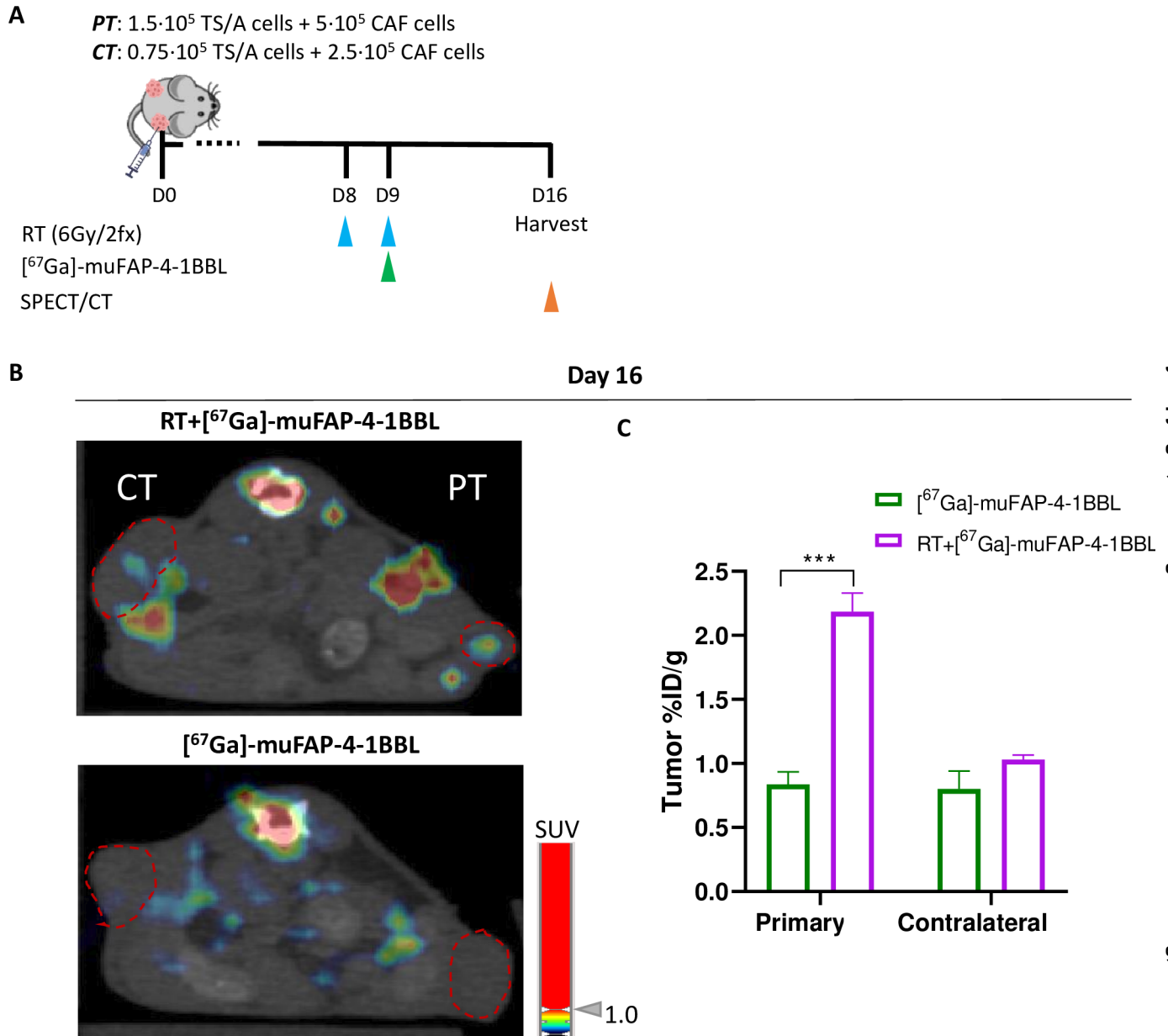


**Figure 5** Radiotherapy enhances muFAP-4-1BBL targeting irradiated tumors. (A) Schematic representation of radiolabeling assay in which muFAP-4-1BBL was labeled with  $^{67}\text{Ga}$  and administered intraperitoneally at day 9 (green arrow) into TS/A+CAF tumor-bearing mice treated or non-treated with RT therapy (RT, blue arrows) of the primary tumor (PT) but not contralateral tumor (CT). Biodistribution analysis measuring radioactivity was performed by SPECT/CT images obtained *in vivo* on day 16 (orange arrows). (B) Representative SPECT/CT images of mice at day 16 of muFAP-4-1BBL monotherapy and RT+muFAP-4-1BBL where the PT was irradiated. The coronal section of mice is shown on SPECT/CT images. The red dotted circles are indicating the location of the CT and PT. (C) Ex vivo biodistribution analysis performed by gamma counter and displayed as per cent of injected dose per gram of tumor (%ID/g) of both primary and contralateral tumors of indicated mice ( $n=3$  mice/group, mean $\pm$ SEM) (two-way analysis of variance); \*\*\* $p<0.001$ . CAF, cancer-associated fibroblast; FAP, fibroblast activation protein; RT, radiotherapy.

### Combination of systemic PD-1 and CTLA-4 checkpoint inhibitors with muFAP-4-1BBL synergize with radiotherapy achieving curative abscopal effects

With the aim of improving the abscopal effects and to control non-irradiated CTs, immunotherapy agents used in the clinic such as anti-PD-1 and anti-CTLA-4 antibodies were tested in combination with the current RT+muFAP-4-1BBL combination (figure 6A). A bilateral TS/A tumor experiment was performed,

starting treatment as late as day+10 after tumor cell engraftment to extend the therapeutic window. The synergy between RT and the anti-CTLA-4 plus anti-PD-1 combination regimen was studied to demonstrate the therapeutic potential of this strategy. The addition of anti-PD-1 slightly increased the response but anti-CTLA-4 greatly improved the outcome in both irradiated and non-irradiated concomitant tumors. Importantly, the quadruple combination cured all

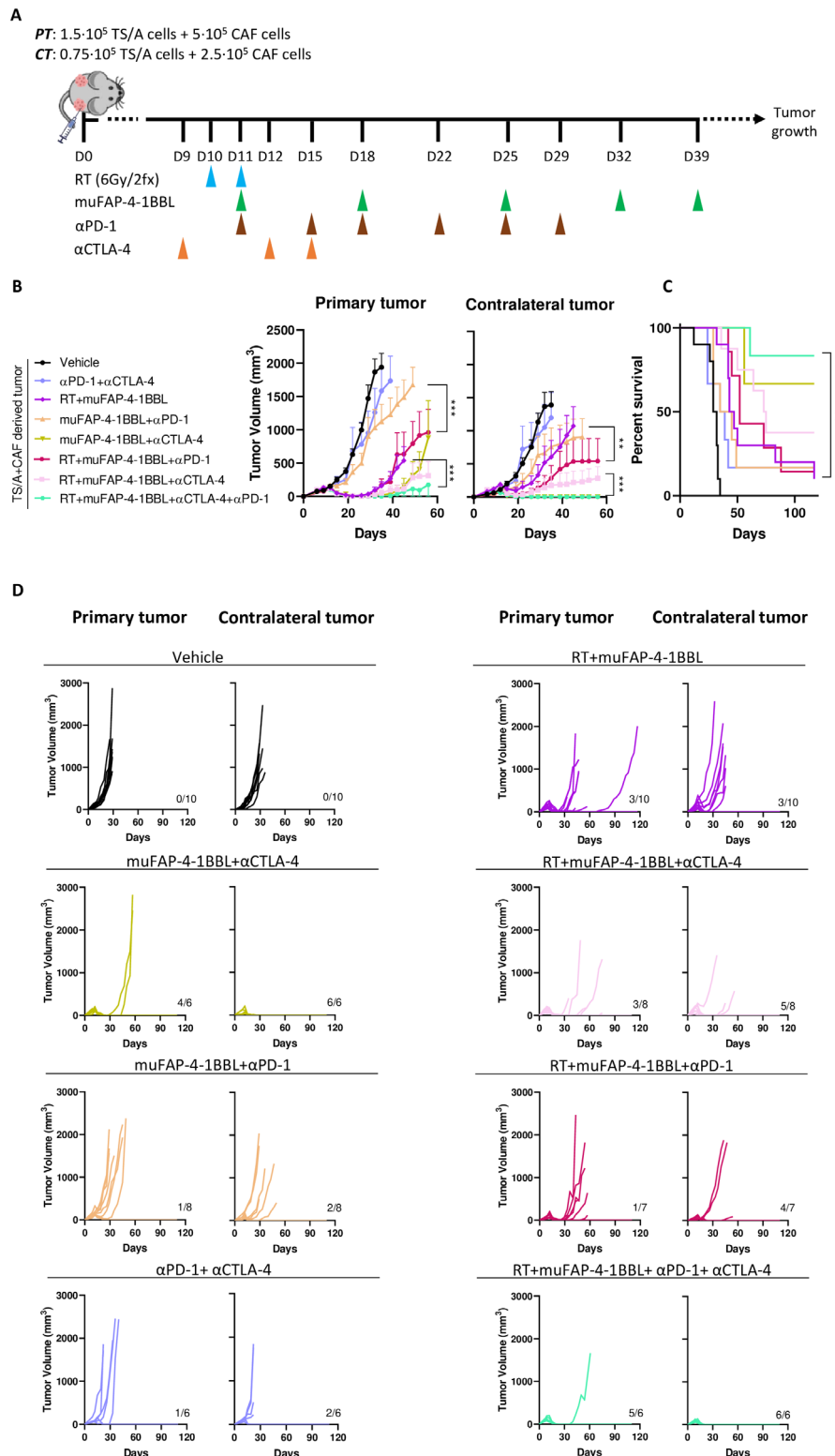


**Figure 6** Combinations of systemic PD-1 and CTLA-4 blockade with muFAP-4-1BBL further synergize with radiotherapy to attain curative abscopal effects. (A) Scheme of 10-day tumor co-engraftment and subsequent treatments of TS/A+CAF tumor-bearing mice with hypofractionated radiotherapy (RT, blue arrows) of the primary tumor (PT) but not contralateral tumor (CT). For combination treatment mice received intraperitoneal administration of muFAP-4-1BBL (green arrows) alone or combined with anti-CTLA-4 (orange arrows) or anti-PD-1 (brown arrows). (B) Tumor growth was monitored and means $\pm$ SEM are shown over time of primary (left) and contralateral tumor (right) (two-way analysis of variance); \*\* $p < 0.01$ , \*\*\* $p < 0.001$ . (C) The percentage of survival over time is shown for experiments in B (Mantel-Cox test); \*\* $p < 0.01$ . (D) Individual tumor sizes of the RT-treated primary tumor and distant non-irradiated contralateral tumors receiving additional treatment as indicated ( $n = 6-10$  mice/group). Pooled data from two independent experiments. CAF, cancer-associated fibroblast; CTLA-4, cytotoxic T-lymphocyte associated protein 4; FAP, fibroblast activation protein; PD-1, programmed cell death protein-1.

CTs therefore achieving eradicated abscopal effects (figure 6B–D). By contrast, muFAP-4-1BBL in combination with anti-CTLA-4, without anti-PD-1, cured the CTs but not the primary ones and showed observable efficacy only against smaller size tumors in the TS/A+CAF tumor model.

### Radiotherapy upregulates FAP expression in the tissue of patients with colorectal carcinoma

From a cohort of patients with colon carcinoma receiving CRT followed by surgery, baseline biopsies and tumor resections (post-CRT) were analyzed using immunohistochemistry and multiplex immunofluorescence imaging (figure 7A and online supplemental figures 8; 9). The densities of T cells (CD3<sup>+</sup>), cytotoxic T cells (CD3<sup>+</sup>CD8<sup>+</sup>), and cancer-associated fibroblast (FAP<sup>+</sup> CAF) were increased after radiation when compared with the corresponding baseline pretreatment biopsy (figure 7B). Notably, increased densities of T cells and FAP<sup>+</sup> CAFs were observed in both the tumor bed and peritumoral tissue of patients with complete pathological responses, while this was not seen in patients with residual disease (figure 7B–C, online supplemental figure 8). These translational results in human patients support that irradiation enriches the presence of FAP-expressing CAFs in the TME and warrants clinical trials to test the FAP-4-1BBL construct, which has already been safely tested in the clinic,<sup>38</sup> in combination with RT.

### DISCUSSION

This study provides a rationale to combine RT with FAP targeting antibodies even in metastatic disease settings in which not all tumor lesions can be irradiated. We showed that hypofractionated RT with two doses of 6 Gy increases the numbers of FAP<sup>+</sup> CAFs within TME. In order to elucidate the origin of FAP-expressing fibroblasts, CAF-GFP<sup>+</sup> were co-injected with TS/A malignant cells. Although tumors showed clearance of co-injected CAFs, there was an important recruitment of endogenous FAP<sup>+</sup> CAFs (GFP<sup>+</sup>) following tumor irradiation, suggesting that irradiation modulates the TME to recruit activated CAFs into the tumor. In addition, in the TS/A tumor model without CAF inoculation, we did not observe any increase in FAP<sup>+</sup> CAFs. This result raises the notion that exogenous CAF inoculation is important in our model for RT to exploit FAP-4-1BBL mediated response. A cross-talk between exogenous CAFs and endogenous CAF for further recruitment could be an explanation. It is important to note that there is no canonical marker to identify all CAFs, and FAP expression is not exclusive to this population.<sup>39</sup> In our experiments, we used additional markers such as  $\alpha$ SMA and collagen type VI alongside FAP for CAF identification (online supplemental figure 9). However, to draw stronger conclusions regarding irradiation-induced recruitment of FAP<sup>+</sup> CAFs, further studies in other tumor types would be valuable.

Moreover, the observed augmented FAP presence explains the enhanced tumor targeting of <sup>67</sup>Ga radiolabeled muFAP-4-1BBL shown after local tumor irradiation since in the non-irradiated CT, targeting was similar to controls. In addition, no liver toxicity was observed, which was the reason for the superagonist anti-4-1BB urelumab to stop clinical development at effective doses.<sup>40,41</sup> muFAP-4-1BBL fusion protein, apart from targeting 4-1BB agonism to TME by FAP binding moiety, mutations on the Fc region were performed to avoid Fc $\gamma$ R binding-derived liver toxicity.<sup>27</sup> In relation to these issues, we analyzed liver accumulation measuring <sup>67</sup>Ga radiolabeled muFAP-4-1BBL and muDP47-4-1BBL fusion proteins. Interestingly, FAP-4-1BBL competes with endogenous expressed 4-1BBL including endogenous soluble 4-1BBL, whereas urelumab is non-4-1BBL competing. Therefore FAP-4-1BBL differs in epitope binding to 4-1BB and lacks Fc-mediated cross-linking at difference with urelumab, as these two factors have been incriminated for urelumab-mediated liver toxicity.<sup>42</sup>

In vivo studies were performed with RT combined with muFAP-4-1BBL antibody fusion protein, showing local efficacy and detectable partial abscopal responses yet of modest intensity. Interestingly, muDP47-4-1BBL did show a slight efficacy in local and CTs when this construct is not cross-linked. An explanation for the modest but measurable efficacy of muDP47-4-1BBL could be that RT-induced cell death-related may favor the binding of DP47 and enable crosslinking and thereby 4-1BB stimulation.<sup>43</sup> RT is also known to induce a certain degree of immunogenic cell death,<sup>44,45</sup> releasing damage associated molecular patterns (DAMPs) that stimulate pattern recognition receptor (PRR) expressed by innate immune cells to mount or amplify antitumor immune responses.

TME remodeling on combined RT+muFAP-4-1BBL treatment was observed to be conducive towards a more immune-stimulating landscape. Increased infiltration by CD8 and DC was observed together with evidence for increases in activated T cells showing enhanced expression of effector markers. However, increased Treg also suggests some level of induced immunosuppression that prompts our current interest in studying other immune cells associated to by radiation such as myeloid-derived suppressor cells or tumor associated macrophages (TAMs).<sup>46,47</sup> It has already been reported, that the combination of irradiation with agonistic anti-mouse 4-1BB IgG mAb causes an immune-stimulated TME.<sup>48</sup> The anti-tumor therapeutic response was also found to be IFN- $\gamma$  and conventional type 1 dendritic cell (cDC1) dependent. These results go in line with our observations on lymphocyte depletion studies and with the genes upregulated on combination therapy as shown by comparative bulk RNA-seq. Interestingly, the transforming growth factor- $\beta$  (TGF- $\beta$ ) genes (*tgfb2* and *tgfb3*) were downregulated in the combination RT+muFAP-4-1BBL therapy as compared with RT or muFAP-4-1BBL single treatments. Of important note, TGF- $\beta$  is known to be part of radiation-induced fibrosis and one of the downstream

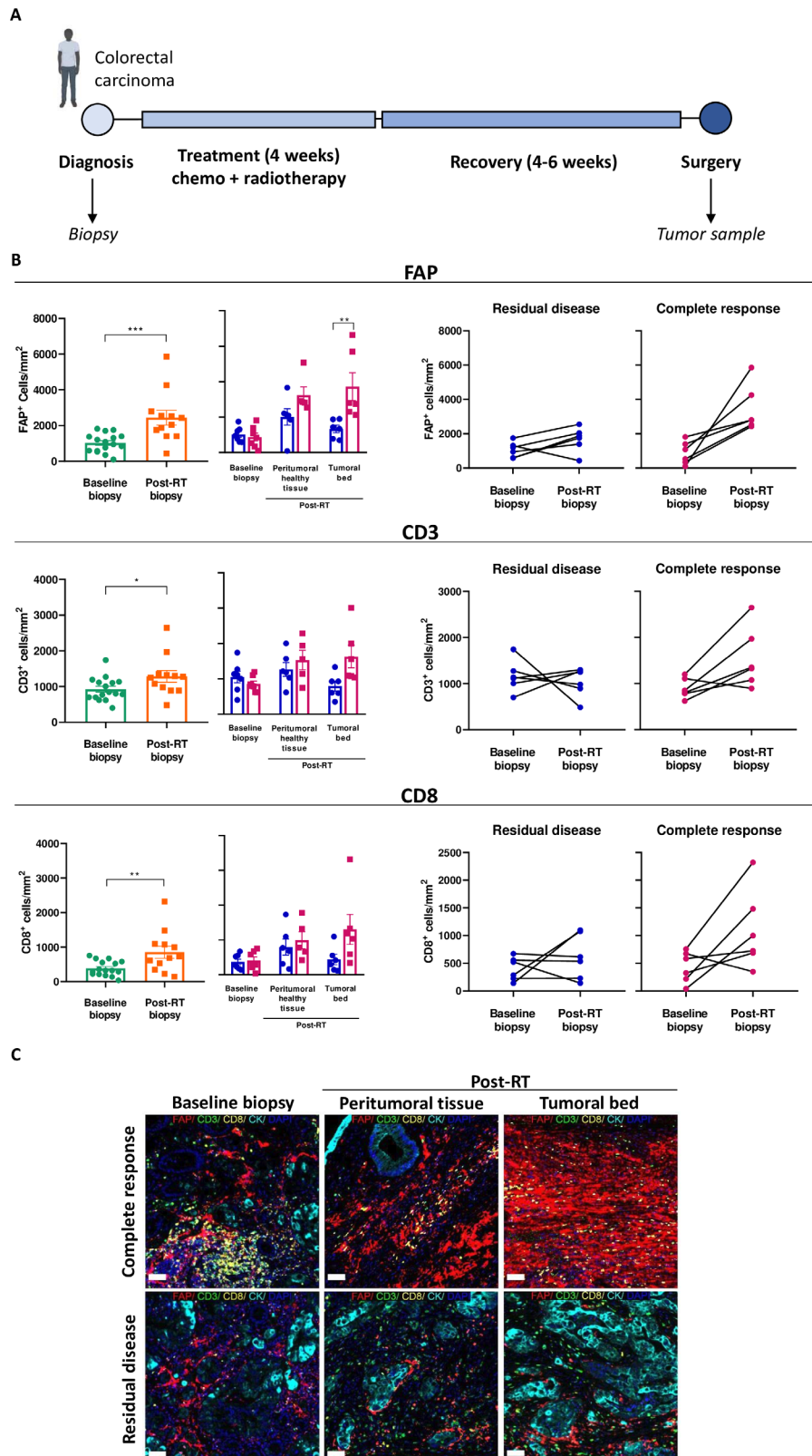


**Figure 7** Post-chemoradiotherapy upregulation of FAP expression in patient-derived colorectal carcinoma tissue samples. (A) Schematic representation of patients with colorectal carcinoma's treatment course from diagnosis, baseline biopsy collection, chemoradiotherapy (CRT) treatment to surgery and post-CRT specimen collection for multiplex immunofluorescence studies (n=12 patients). (B) Plots showing FAP expression and immune infiltration of CD8 and CD3 expressing cells between baseline biopsy and post-CRT specimens in patients with residual disease or complete response evaluated by immunofluorescence imaging of tissue. Each symbol represents one patient, means±SEM are indicated (paired t-test and repeated measured analysis of variance) \*p<0.05, \*\*p<0.01, \*\*\*p<0.001. (C) Immunofluorescence representative images of tumor samples (scale bar 20 µm). FAP, fibroblast activation protein; RT, radiotherapy.

immunosuppressive cytokines unleashed by irradiation. In addition, some reports<sup>49</sup> have linked TGF- $\beta$  with myofibroblastic CAF (myCAF) and extracellular matrix (ECM) deposition.<sup>49</sup> It is tempting to speculate that RT+muFAP-4-1BBL therapy might be counteracting the immunosuppressive CAF phenotype perhaps mitigating the effect of TGF- $\beta$ . Moreover, previously published experiments in mice indicate that TGF- $\beta$  neutralization might be a suitable combination for 4-1BB costimulation and RT.<sup>50</sup>

RT plays a crucial role in the treatment of locally advanced cancers. To corroborate our mouse experimentation in vivo findings, we selected a clinical cohort of colorectal tumors as their standard of care for these patients aligns with the therapeutic approach explored in our study. This cohort included patients with colorectal cancer with distinct pathological outcomes: (1) those with a complete response, exhibiting no residual tumor cells, and (2) those who did not respond well to CRT, presenting residual tumor tissue at surgery. Notably, in this collection of paired baseline and post-CRT biopsies, we observed that radiation increased the presence of FAP<sup>+</sup> cells in colorectal cancer tissue. While these in vivo observations in breast tumors were mirrored in the colorectal cohort, further clinical studies in patients with breast cancer will further be necessary to assess the transferability of these findings even if in breast cancer the surgical bed rather than the tumor is irradiated. Interestingly, these increases were more prominent in tumors with a complete pathological response and were associated with a higher infiltration of T cells, particularly cytotoxic T cells. This suggests that the spatial relationship between FAP expression and areas of complete response—where no residual tumor cells were detected—may reflect radiation-induced fibrosis (scarring).<sup>51</sup> Moreover, this spatial association was also evident in tumors that did not respond well to chemoradiation, raising critical questions about the predominant CAF subtypes in non-responsive tumors. Future studies will explore other CAF subtypes using established markers such as  $\alpha$ SMA or subtype-specific markers (PDPN, ACTA2, FSP1) to deepen our understanding of CAF heterogeneity.<sup>52</sup> To date, several studies have employed multiplex and/or multispectral imaging for CAF characterization and further subclassification.<sup>53 54</sup> Based on our findings, we propose that the combination of RT with FAP-4-1BBL could enhance T-cell activation and CAF recruitment, potentially benefiting tumors with a CAF-rich TME or those showing radiation-induced FAP modulation. Thus, a clinical evaluation in patients with partial RT responses could help define and validate molecular characteristics, such as TGF- $\beta$  presence or specific CAF subtypes, that may optimize the effectiveness of FAP-4-1BBL therapy post-RT. This FAP profile-based approach in the TME could help guide patient selection, personalizing treatment for those most likely to benefit.

Recent studies employing spatial transcriptomics and scRNA-seq have revealed significant diversity among FAP<sup>+</sup> CAFs and their spatial organization in breast cancer.<sup>47</sup> For

instance, one study identified a specific FAP<sup>+</sup> CAF subtype, Detox-iCAF, associated with an immuno-protective niche, while another subtype, ECM-myCAF (another FAP<sup>+</sup> CAF subtype), was linked to an immune-suppressive environment. This crosstalk between CAFs, cancer cells, and immune cells highlights the capacity of CAFs to influence the TME and shape immune responses. Notably, CD8<sup>+</sup> T cells were found predominantly in peritumoral areas, suggesting that CAFs may serve as a physical barrier to effector immune cell infiltration.<sup>47</sup> Similar observations in the stromal microenvironment of melanoma further emphasize this point, where the “stromal barrier” limits access for cancer-infiltrating lymphocytes to tumor cells.<sup>55</sup> Furthermore, it is possible that human colorectal tumors, particularly those subjected to irradiation, might express even higher levels of FAP due to radiation-induced scarring, which could enhance the therapeutic benefit of combining FAP-targeting antibodies with RT. In this context, it is crucial to consider how irradiation may alter CAF behavior. Investigating the non-immune roles that CAFs may adopt following irradiation in our TS/A+CAF model could provide valuable insights. Notably, fibrotic reactions, common undesirable side effects of RT, may play a significant role in shaping these functions and warrant further exploration.

There are data from a human phase I study that confirm the safety and evaluate the efficacy of RO7122290, a bispecific FAP-4-1BBL antibody fusion protein, in combination with atezolizumab in patients with advanced solid tumors.<sup>52</sup> Hence a clinical trial testing the combination of with irradiation is warranted based on safety and the preclinical efficacy results of the combination reported herein. Such a trial should ideally optimize the sequencing of the treatments and consider other additional agents such as checkpoint inhibitors in sequential or concomitant combination regimes.<sup>53</sup>

#### Author affiliations

<sup>1</sup>Department of Immunology and Immunotherapy, Center for Applied Medical Research (CIMA), Pamplona, Spain

<sup>2</sup>Department of Pathology, Cancer Center Clinica Universidad de Navarra, Pamplona, Spain

<sup>3</sup>Department of Immunology, Hospital Gregorio Marañón, Madrid, Madrid, Spain

<sup>4</sup>Roche Innovation Centre Zurich, Roche Pharma Research and Early Development (pRED), Schlieren, Switzerland

<sup>5</sup>Institute of Immunology and Transplantation, University College London, London, UK

<sup>6</sup>Department of Nuclear Medicine, Clinica Universidad de Navarra, Pamplona, Spain

<sup>7</sup>Nuffield Department of Medicine, University of Oxford, Oxford, UK

<sup>8</sup>Departments of Immunology-Immunotherapy and Radiation Oncology, Cancer Center Clinica Universidad de Navarra, Pamplona, Navarra, Spain

<sup>9</sup>Centro de Investigación Biomédica en Red de Cáncer (CIBERONC), Madrid, Spain

<sup>10</sup>Institute for Health Research (IDISNA), Pamplona, Spain

X Eneko Garate-Soraluze @garateeneko, Celia Barrio-Alonso @isgonnabethecel and Alvaro Teijeira @itlive

**Acknowledgements** We are grateful to D Allignani from the flow cytometry facility, to Eneko Elizalde and Elena Ciordia from the animal facility for their excellent work and to Elizabeth Guruceaga from Bioinformatics facility Marga Ecay from nuclear Medicine. Haizea Etxeberria and Sara Fadrique for excellent dosimetry. Drs Labiano, Aranda and Berraondo are acknowledged for helpful discussions.

**Contributors** MER-R designed experiments, supervised the project, analyzed results, and wrote the article. EG-S performed experiments, analyzed results, and wrote the article. IS-M and LF-R performed experiments, analyzed results and edited the manuscript. IM designed experiments, co-supervised the project and wrote the article. All authors have read and agreed to the published version of the manuscript. CC designed and produced muFAP-4-1BBL and muDP47-4-1BBL. CC performed functional quality controls before shipment. CK, CC, TT and PU provided input into the project and study design and revised the manuscript. MER-R acts as guarantors.

**Funding** This work has been supported by the imCORE Network on behalf of F. Hoffmann-La Roche (NAV-11 project). MER-R is supported by the CRIS investigator grant (PR\_TCL\_2020-3). EG-S is supported by a predoctoral grant from the Scientific Foundation of the Spanish Association Against Cancer (PRDNA234014GARA).

**Competing interests** EG-S, IS-M, LF-R, AR, CEDA, CB-A, CdPH, CLR, AT, JAS, MC, and PS-M declare no competing interests. MER-R reports receiving research funding from Roche and Highlight Therapeutics. She also has received speaker's bureau honoraria from BMS and ROCHE. IM reports receiving commercial research grants from BMS, Highlight Therapeutics, Alligator, Pfizer Genmab and Roche; has received speaker's bureau honoraria from MSD; and is consultant or advisory board member for BMS, Roche, AstraZeneca, Genmab, Pharmamar, F-Star, Bioncotech, Bayer, Numab, Pieris, Gossamer, Alligator and Merck Serono. CK, PU, CC, and TT declare employment, stock ownership and patents with Roche.

**Patient consent for publication** Not applicable.

**Ethics approval** This study involves human participants and was approved by Ethics Committee of the University of Navarra. Project code 2010.111 mod4. Participants gave informed consent to participate in the study before taking part.

**Provenance and peer review** Not commissioned; externally peer reviewed.

**Data availability statement** All data relevant to the study are included in the article or uploaded as supplementary information.

**Supplemental material** This content has been supplied by the author(s). It has not been vetted by BMJ Publishing Group Limited (BMJ) and may not have been peer-reviewed. Any opinions or recommendations discussed are solely those of the author(s) and are not endorsed by BMJ. BMJ disclaims all liability and responsibility arising from any reliance placed on the content. Where the content includes any translated material, BMJ does not warrant the accuracy and reliability of the translations (including but not limited to local regulations, clinical guidelines, terminology, drug names and drug dosages), and is not responsible for any error and/or omissions arising from translation and adaptation or otherwise.

**Open access** This is an open access article distributed in accordance with the Creative Commons Attribution Non Commercial (CC BY-NC 4.0) license, which permits others to distribute, remix, adapt, build upon this work non-commercially, and license their derivative works on different terms, provided the original work is properly cited, appropriate credit is given, any changes made indicated, and the use is non-commercial. See <http://creativecommons.org/licenses/by-nc/4.0/>.

#### ORCID iDs

Eneko Garate-Soraluze <http://orcid.org/0000-0002-4071-1427>  
 Celia Barrio-Alonso <http://orcid.org/0000-0002-2789-1363>  
 Alvaro Teijeira <http://orcid.org/0000-0002-7339-4464>  
 Christian Klein <http://orcid.org/0000-0001-7594-7280>  
 Ignacio Melero <http://orcid.org/0000-0002-1360-348X>  
 Maria E Rodriguez-Ruiz <http://orcid.org/0000-0002-9765-2499>

#### REFERENCES

- Kalluri R. The biology and function of fibroblasts in cancer. *Nat Rev Cancer* 2016;16:582–98.
- Orimo A, Weinberg RA. Stromal fibroblasts in cancer: a novel tumor-promoting cell type. *Cell Cycle* 2006;5:1597–601.
- Kalluri R, Zeisberg M. Fibroblasts in cancer. *Nat Rev Cancer* 2006;6:392–401.
- Paulsson J, Micke P. Prognostic relevance of cancer-associated fibroblasts in human cancer. *Semin Cancer Biol* 2014;25:61–8.
- Hellevik T, Pettersen I, Berg V, et al. Changes in the Secretary Profile of NSCLC-Associated Fibroblasts after Ablative Radiotherapy: Potential Impact on Angiogenesis and Tumor Growth. *Transl Oncol* 2013;6:66–74.
- Nazareth MR, Broderick L, Simpson-Abelson MR, et al. Characterization of human lung tumor-associated fibroblasts and their ability to modulate the activation of tumor-associated T cells. *J Immunol* 2007;178:5552–62.
- Takahashi H, Sakakura K, Kudo T, et al. Cancer-associated fibroblasts promote an immunosuppressive microenvironment through the induction and accumulation of protumoral macrophages. *Oncotarget* 2016;8:8633–47.
- Servais C, Erez N. From sentinel cells to inflammatory culprits: cancer-associated fibroblasts in tumour-related inflammation. *J Pathol* 2013;229:198–207.
- Harper J, Sainson RCA. Regulation of the anti-tumour immune response by cancer-associated fibroblasts. *Semin Cancer Biol* 2014;25:69–77.
- Wang Z, Yang Q, Tan Y, et al. Cancer-Associated Fibroblasts Suppress Cancer Development: The Other Side of the Coin. *Front Cell Dev Biol* 2021;9:613534.
- Greimelmaier K, Klopp N, Mairinger E, et al. Fibroblast activation protein- $\alpha$  expression in fibroblasts is common in the tumor microenvironment of colorectal cancer and may serve as a therapeutic target. *Pathol Oncol Res* 2023;29:1611163.
- Herrera M, Mezheyeuski A, Villabona L, et al. Prognostic Interactions between FAP+ Fibroblasts and CD8a+ T Cells in Colon Cancer. *Cancers (Base)* 2020;12:3238.
- Wong KY, Cheung AHK, Chen B, et al. Cancer-associated fibroblasts in nonsmall cell lung cancer: From molecular mechanisms to clinical implications. *Int J Cancer* 2022;151:1195–215.
- Costa A, Kieffer Y, Scholer-Dahirel A, et al. Fibroblast Heterogeneity and Immunosuppressive Environment in Human Breast Cancer. *Cancer Cell* 2018;33:463–79.
- Hu D, Li Z, Zheng B, et al. Cancer-associated fibroblasts in breast cancer: Challenges and opportunities. *Cancer Commun (Lond)* 2022;42:401–34.
- Homicksko K, Barras D, Lopez VA, et al. Unsorted single-cell RNA sequencing profiles of metastatic melanoma patients reveal the heterogeneity of melanoma-associated fibroblasts. *Ann Oncol* 2019;30:v536.
- Chen M, Xiao L, Jia H, et al. Stereotactic ablative radiotherapy and FAP $\alpha$ -based cancer vaccine suppresses metastatic tumor growth in 4T1 mouse breast cancer. *Radiother Oncol* 2023;189:109946.
- Nadal L, Peissert F, Elsayed A, et al. Generation and *in vivo* validation of an IL-12 fusion protein based on a novel anti-human FAP monoclonal antibody. *J Immunother Cancer* 2022;10:e005282.
- Rivas EI, Linares J, Zwick M, et al. Targeted immunotherapy against distinct cancer-associated fibroblasts overcomes treatment resistance in refractory HER2+ breast tumors. *Nat Commun* 2022;13:5310.
- Labiano S, Roh V, Godfroid C, et al. CD40 Agonist Targeted to Fibroblast Activation Protein  $\alpha$  Synergizes with Radiotherapy in Murine HPV-Positive Head and Neck Tumors. *Clin Cancer Res* 2021;27:4054–65.
- Waldhauer I, Gonzalez-Nicolini V, Freimoser-Grundschober A, et al. Simlukafusp alfa (FAP-IL2v) immunocytokine is a versatile combination partner for cancer immunotherapy. *MAbs* 2021;13:1913791.
- Trüb M, Uhlenbrock F, Claus C, et al. Fibroblast activation protein-targeted-4-1BB ligand agonist amplifies effector functions of intratumoral T cells in human cancer. *J Immunother Cancer* 2020;8:e000238.
- Martinez-Zubiaurre I, Chalmers AJ, Hellevik T. Radiation-Induced Transformation of Immunoregulatory Networks in the Tumor Stroma. *Front Immunol* 2018;9:1679.
- Yang X, Lin Y, Shi Y, et al. FAP Promotes Immunosuppression by Cancer-Associated Fibroblasts in the Tumor Microenvironment via STAT3–CCL2 Signaling. *Cancer Res* 2016;76:4124–35.
- Li M, Cheng X, Rong R, et al. High expression of fibroblast activation protein (FAP) predicts poor outcome in high-grade serous ovarian cancer. *BMC Cancer* 2020;20:1032.
- Jia Z, Ragoonanan D, Mahadeo KM, et al. n.d. IL12 immune therapy clinical trial review: Novel strategies for avoiding CRS-associated cytokines. *Front Immunol* 2013.
- Claus C, Ferrara C, Xu W, et al. Tumor-targeted 4-1BB agonists for combination with T cell bispecific antibodies as off-the-shelf therapy. *Sci Transl Med* 2019;11:eaa5989.
- Lo M, Kim HS, Tong RK, et al. Effector-attenuating Substitutions That Maintain Antibody Stability and Reduce Toxicity in Mice. *J Biol Chem* 2017;292:3900–8.
- Abengozar-Muela M, Esparza MV, Garcia-Ros D, et al. Diverse immune environments in human lung tuberculosis granulomas assessed by quantitative multiplexed immunofluorescence. *Mod Pathol* 2020;33:2507–19.

- 30 López-Janeiro Á, Villalba-Esparza M, Brizzi ME, *et al.* The association between the tumor immune microenvironments and clinical outcome in low-grade, early-stage endometrial cancer patients. *J Pathol* 2022;258:426–36.
- 31 Bolger AM, Lohse M, Usadel B. Trimmomatic: a flexible trimmer for Illumina sequence data. *Bioinformatics* 2014;30:2114–20.
- 32 Dobin A, Davis CA, Schlesinger F, *et al.* STAR: ultrafast universal RNA-seq aligner. *Bioinformatics* 2013;29:15–21.
- 33 Liao Y, Smyth GK, Shi W. featureCounts: an efficient general purpose program for assigning sequence reads to genomic features. *Bioinformatics* 2014;30:923–30.
- 34 Frankish A, Diekhans M, Ferreira A-M, *et al.* GENCODE reference annotation for the human and mouse genomes. *Nucleic Acids Res* 2019;47:D766–73.
- 35 Robinson MD, McCarthy DJ, Smyth GK. edgeR: a Bioconductor package for differential expression analysis of digital gene expression data. *Bioinformatics* 2010;26:139–40.
- 36 Ritchie ME, Phipson B, Wu D, *et al.* limma powers differential expression analyses for RNA-seq and microarray studies. *Nucleic Acids Res* 2015;43:e47.
- 37 Yu G, Wang LG, Han Y, *et al.* clusterProfiler: an R package for comparing biological themes among gene clusters. *OMICS* 2012;16:284–7.
- 38 Rodríguez-Ruiz ME, Serrano-Mendioroz I, Garate-Soraluze E, *et al.* Intratumoral BO-112 in combination with radiotherapy synergizes to achieve CD8 T-cell-mediated local tumor control. *J Immunother Cancer* 2023;11:e005011.
- 39 Tommelein J, De Vlieghere E, Verset L, *et al.* Radiotherapy-Activated Cancer-Associated Fibroblasts Promote Tumor Progression through Paracrine IGF1R Activation. *Cancer Res* 2018;78:659–70.
- 40 Melero I, Sanmamed MF, Glez-Vaz J, *et al.* CD137 (4-1BB)-Based Cancer Immunotherapy on Its 25th Anniversary. *Cancer Discov* 2023;13:552–69.
- 41 Etxeberria I, Glez-Vaz J, Teijeira Á, *et al.* New emerging targets in cancer immunotherapy: CD137/4-1BB costimulatory axis. *ESMO Open* 2020;4:e000733.
- 42 Ho SK, Xu Z, Thakur A, *et al.* Epitope and Fc-Mediated Cross-linking, but Not High Affinity, Are Critical for Antitumor Activity of CD137 Agonist Antibody with Reduced Liver Toxicity. *Mol Cancer Ther* 2020;19:1040–51.
- 43 Glez-Vaz J, Azpilikueta A, Ochoa MC, *et al.* CD137 (4-1BB) requires physically associated cIAPs for signal transduction and antitumor effects. *Sci Adv* 2023;9:eadf6692.
- 44 Galassi C, Klapp V, Formenti SC, *et al.* Immunologically relevant effects of radiation therapy on the tumor microenvironment. *Essays Biochem* 2023;67:979–89.
- 45 Rodríguez-Ruiz ME, Vanpouille-Box C, Melero I, *et al.* Immunological Mechanisms Responsible for Radiation-Induced Abscopal Effect. *Trends Immunol* 2018;39:644–55.
- 46 Wang L, Dou X, Chen S, *et al.* YTHDF2 inhibition potentiates radiotherapy antitumor efficacy. *Cancer Cell* 2023;41:1294–308.
- 47 Croizer H, Mhaidly R, Kieffer Y, *et al.* Deciphering the spatial landscape and plasticity of immunosuppressive fibroblasts in breast cancer. *Nat Commun* 2024;15:2806.
- 48 Rodríguez-Ruiz ME, Rodríguez I, Garasa S, *et al.* Abscopal Effects of Radiotherapy Are Enhanced by Combined Immunostimulatory mAbs and Are Dependent on CD8 T Cells and Crosspriming. *Cancer Res* 2016;76:5994–6005.
- 49 Perez-Penco M, Weis-Banke SE, Schina A, *et al.* TGFβ-derived immune modulatory vaccine: targeting the immunosuppressive and fibrotic tumor microenvironment in a murine model of pancreatic cancer. *J Immunother Cancer* 2022;10:e005491.
- 50 Rodríguez-Ruiz ME, Rodríguez I, Mayorga L, *et al.* TGFβ Blockade Enhances Radiotherapy Abscopal Efficacy Effects in Combination with Anti-PD1 and Anti-CD137 Immunostimulatory Monoclonal Antibodies. *Mol Cancer Ther* 2019;18:621–31.
- 51 Nguyen HQ, To NH, Zadigue P, *et al.* Ionizing radiation-induced cellular senescence promotes tissue fibrosis after radiotherapy. A review. *Crit Rev Oncol Hematol* 2018;129:13–26.
- 52 Melero I, Tanos T, Bustamante M, *et al.* A first-in-human study of the fibroblast activation protein-targeted, 4-1BB agonist RO7122290 in patients with advanced solid tumors. *Sci Transl Med* 2023;15:eabp9229.
- 53 Sanmamed MF, Berraondo P, Rodríguez-Ruiz ME, *et al.* Charting roadmaps towards novel and safe synergistic immunotherapy combinations. *Nat Cancer* 2022;3:665–80.
- 54 Gunasekaran K, Pentony M, Shen M, *et al.* Enhancing antibody Fc heterodimer formation through electrostatic steering effects: applications to bispecific molecules and monovalent IgG. *J Biol Chem* 2010;285:19637–46.
- 55 Bitra A, Doukov T, Destito G, *et al.* Crystal structure of the m4-1BB/4-1BBL complex reveals an unusual dimeric ligand that undergoes structural changes upon 4-1BB receptor binding. *J Biol Chem* 2019;294:1831–45.